Growth and Favorable Bioelectrocatalysis of Multishaped Nanocrystal Au in Vertically Aligned TiO_2 Nanotubes for Hemoprotein

Guohua Zhao,* Yanzhu Lei, Yonggang Zhang, Hongxu Li, and Meichuan Liu

Department of Chemistry, Tongji University, Shanghai 200092, China

Received: December 24, 2007; Revised Manuscript Received: June 21, 2008

A novel nanostructure noble metal-TiO_2 nanotube composite electrode was constructed for effective immobilization of cytochrome *c* (Cyt *c*) and successful realization of its direct electrochemistry and electrocatalysis. Highly ordered and vertically aligned TiO_2 nanotubes (NTs) successfully in situ grew on titanium substrate by anodic oxidation of Ti, possessing large surface areas and a high aspect ratio of nanotubular structure. They can be used as excellent templates. Au nanocrystal (Au NCs) were subsequently introduced into the TiO_2 NTs by one-step electrodeposition to form AuNCs-TiO_2 NTs hybrids, aiming at enhancing the electrochemical performance and biocompatibility of the electrode. The formation mechanism of the Au NCs was elucidated from field-emission scanning electron microscopy (SEM) and X-ray diffraction (XRD) character. Au NCs could grow to different shaped nanostructures such as polyhedral nanorods with high-index facets, honey-cave-like nanocages, etc., due to the tubular confinement of the TiO_2 NTs. Experimental results also indicated that this novel nanocomposite electrode provided a good environment for protein immobilization and biosensor preparation. The multishapes of Au NCs resulted in better promotion for direct electrochemistry and fast electron transfer of Cyt *c* on the Au NCs-TiO_2 NTs composite electrode, either immobilized on the electrode or dissolved in solutions. The immobilized Cyt *c* exhibited favorable electrocatalytic activity toward the reduction of H_2O_2 with good stability and sensitivity. The linear range was 2×10^{-6} to 3.49×10^{-4} mol·L^{-1}, with a detection limit of 1.21×10^{-6} mol·L^{-1}. Moreover, it could be adapted to different pH circumstances, ranging from 3 to 8, with good response and resolution. This makes the AuNCs-TiO_2 NTs composite electrode a promising platform for fabricating third-generation biosensors.

1. Introduction

It is well-known that the microscale, microstructure, and modified species of a material have a close relationship with its electrochemical properties and the electrochemical reaction on its surface. Some important elements, including the three-dimension geometric structure, the orientation and exposure of each crystal plane, the specific surface area, and the number of catalyzed active sites, play key roles on the electrochemical performance of the material. Great efforts have been taken to search for advanced fabrication techniques and excellent modified materials with appropriate scales, structures, and surface species.

Nowadays, with the development of nanotechnology, the direct electrochemical reaction of biomolecules such as proteins on the nanostructures electrodes and nanomaterial assembled or modified electrodes has attracted great interest from researchers. The modification or assembly of nanomaterials on the surface of an electrode can facilitate the electron transfer rate of biomolecules directly. A good many nanomaterials have been reported for the immobilization of proteins or enzymes, including a large number of noble metal nanoparticles (NPs),[1−5] carbon nanotubes (CNTs),[5−9] semiconductor quantum dots (QDs),[10,11] micro- or mesoporous zeolite,[12,13] and so on. Among them, nanotubes (NTs) are undoubtedly a sort of novel nanostructure species which possess high ratio surface area and multiple active sites. Reports have specified carbon NTs[6−8,14,15] and silicon NTs,[16] prepared by chemical vapor deposition (CVD) or template synthesis methods, being modified onto glassy carbon electrodes (GCE) or Au electrodes for the direct electrochemistry of macromolecule proteins by means of dropping coat or sol−gel. Recently, TiO_2 NTs have been gradually attracting considerable attention and have become a hot research topic for photocatalysis, photoelectrocatalytic degradation, and gas sensors, due to their unique chemical and physical properties, such as three-dimensional nanostructures, uniform nanochannel, electronic conductivity, good hydrophilicity, larger specific surface area, etc., which may greatly enhance their activity as catalysts or sensitivity.[17−22]

Vast reports have focused on the photoelectric catalysis of TiO_2 NTs.[20−23] At the same time, TiO_2 has also been involved in the bioelectrochemistry field and the development of biosensors because of its chemical inertness, rigidity, thermal stability, nontoxicity, and good biocompatibility. Researches have figured out that electrodes modified with TiO_2 nanofilm exhibit catalysis for biomolecules such as myoglobin (Mb), hemoglobin (Hb), and catalase, without any addition of electron transfer mediators or promoters.[24−27] Other literature indicates that TiO_2 powders can be prepared as tubular structures by hydrothermal treatment in NaOH solution. The as-prepared TiO_2 NTs loaded with biomolecules can further be uniformly cast onto a pyrolytic graphite (PG) disk electrode or GCE, resulting in the bioactivity of the biomolecules being partially maintained and the electrochemical characteristics toward hemoproteins being observed to some degree.[17,28,29]

Furthermore, it is noticeable that vertical TiO_2 NTs in situ growing on Ti substrate can serve as excellent carriers for the further loading or modification of catalyzer species compared

* To whom correspondence should be addressed. E-mail: g.zhao@mail.tongji.edu.cn. Phone: +86-21-65988570-8244. Fax: +86-21-65982287.

10.1021/jp712054c CCC: $40.75
Published on Web 08/29/2008

with TiO_2 nanofilms and nanoparticles. The electro- and photocatalysis performances of highly ordered TiO_2 NTs and relevant modified TiO_2 NTs have been widely reported.[19−21,30−32] Macak et al.[32] deposited Au nanoparticles onto the TiO_2 NTs, and found that they can be used as a highly efficient catalyst system for the electrochemical oxygen reduction reaction in aqueous solutions. Yang et al.[33] electrochemically deposited Co−Ag−Pt inside the nanotubes, and found the catalytic activity increased compared with that of the Pt electrode.

Similarly, if some noble metals with good electrochemistry performance were inlaid in the TiO_2 NTs, it is believed to enhance the electrochemical activity and biocompatibility greatly for them. Therefore, two main points are our concern in the present work. First, the vertically aligned TiO_2 NT array can serve as an excellent template with high surface area ratio and free space. Nanostructure materials with outstanding performance, which are capable of serving as biosensors, can be constructed by filling some noble metal species such as Au with high catalysis competence. The tubular structure and size of TiO_2 NTs can confine and control the growing process of Au in TiO_2 NTs. Thus, Au might grow to a certain size and structure, and accordingly exhibit different electrochemical properties compared with the normal Au disk electrode or TiO_2 NTs. Meanwhile, TiO_2 NTs can provide more active sites for the deposition and dispersion of Au. The diversity of nanostuctured Au may enhance the electrochemical properties at a certain degree compared with Au deposited on a plane electrode. Second, because TiO_2 NTs have different sizes and shapes, Au can grow to different nanostructures, thus can exhibit better promotion for the direct electrochemistry and electron transfer of macromolecular protein in total compared with Au deposited on a plane surface electrode. And the potential application of this nanotube-noble metal composite electrode in biosensing also can be taken into account. To the best of our knowledge, few reports have dealt with such aspects.

In the present paper, TiO_2 NTs were prepared by anodic oxidation of Ti through a simple in situ growth process, and were chosen to construct Au nanocrystals (Au NCs)-TiO_2 NTs composite material. Au was electrodeposited in the TiO_2 NTs, and grew to different nanostructures, forming NCs-NTs hybrid materials. This novel electrode was further applied to catalyze the direct electrochemical redox of protein macromolecules such as cytochrome *c* (Cyt *c*), which is a kind of typical hemoprotein and plays an important role in the biological respiratory chain.[34,35] It is well-known that the voltammetric response of Cyt *c* is quite poor at bare metal electrodes, most likely due to the denaturation of protein on the metal electrode surface, which would lead to extremely slow electron-transfer kinetics. Its direct electrochemical behavior was accordingly hard to observe in solutions, and mediators or promoters were usually needed to promote the electron transfer of Cyt *c*.[2,35,36] But as long as it is immobilized onto the surface of a nanoparticle Au modified electrode, it becomes much easier to observe its voltammetric response.[1,2,4,37] However, in our study, the results indicate that this nanocomposite electrode can promote the direct electrochemical redox of Cyt *c* both immobilized on the electrode and in the solutions. And based on this, a H_2O_2 biosensor was designed with a satisfactory linear range, comparative detection limit, and good sensitivity. Furthermore, experimental results demonstrate that both the tubular structures of TiO_2 NTs arrays and the formed different Au NCs can provide a molecular channel to allow the protein to easily arrive at the electrode surface, and the surfaces of the inner wall of the TiO_2 NTs with good biocompatibility and feasibility of chemical modification retain the activity of the biomaterial to a great extent. A new approach for realizing the direct electrochemistry of proteins, as well as the design of novel bioelectronic devices, has been accordingly provided.

2. Experimental Methods

2.1. Reagents and Apparatus. Horse heart cytochrome *c* was obtained from Sigma (Sigma Co. USA) and used as received. Pure titanium foils (99.9% purity) cut into 1.5 × 4.0 cm^2 pieces were used for anodic oxidation. All the other reagents were of analytical grade and were used without further purification. Bioelectrochemical experiments were carried out in 25 $mmol \cdot L^{-1}$ phosphate buffer solution (PBS). Double-distilled water was used throughout the experiments.

Field emission scanning electron microscope (EFEG-SEM) (Quanta 200 FEG, FEI) and X-ray diffraction (XRD) (Bruker Co., Ltd., Germany) were used to characterize the morphology and crystal structure of the as-prepared electrodes. The surface contact angles were measured with a sessile drop contact angle meter (JC2000A, Zhongchen) at room temperature and ambient humidity. A sessile drop of water or 10 $\mu mol \cdot L^{-1}$ Cyt *c* solution (about 5 μL) was placed carefully onto the as-prepared electrode, using a manual microsyringe fixture. Ultraviolet and visible (UV−vis) absorption spectra were recorded at room temperature with an Aglient 8453 UV−vis spectrophotometer.

2.2. In Situ Growth of Ordered Vertically Aligned TiO_2 NTs on Ti Substrate. TiO_2 NTs based on Ti substrate were fabricated according to the method reported in the literature,[32,38] with a little modification. Titanium foils of 0.80 mm thickness were used as the electrode substrate. Prior to anodic oxidation, the titanium foils were mechanically polished with different emery papers to a mirror-like finish. And then they were ultrasonically cleaned in distilled water and acetone for 20 min, respectively. After being rinsed thoroughly with pure water, the clean titanium foil electrode was first etched in an 18% HCl solution at 85 °C for 10 min. The etched titanium foil was rinsed thoroughly with pure water and then anodized in a 1:8 acetic acid−water solution containing 0.5 vol % hydrofluoric acid at 20 V for 45 min, forming TiO_2 nanotube arrays on the Ti substrate. Finally the as-prepared TiO_2 NTs array was annealed at 500 °C under oxygen ambience for 5 h with a heating and cooling rate of 1 deg/min to obtained stable NTs. For comparison, the Ti electrode was prepared by anodic oxidation in a 1:8 acetic acid−water solution without HF and was also annealed under the same thermal conditions as the nanotubular structures.

2.3. Bottom-to-Top Growth of Au NCs in Vertical TiO_2 NTs. Potentiostatic deposition was carried out to load Au NCs in vertical TiO_2 NTs. In a typical experiment, a three-electrode system was used, with the TiO_2 NTs as the working electrode, a platinum electrode as the counter electrode, and a saturated calomel electrode (SCE) as the reference electrode. Electrodeposition was carried out in 1% (w/w) $HAuCl_4$ + 0.02 $mol \cdot L^{-1}$ H_2SO_4. After deposition, the electrode was immersed into 0.2 $mol \cdot L^{-1}$ HF solution for 30 s to remove the TiO_2 NTs partially. Finally, the as-prepared Au NCs loaded TiO_2 NTs, which we defined as the Au NCs-TiO_2 NTs/Ti electrode, was rinsed thoroughly with distilled water. For comparison, Au was also directly electrodeposited onto Ti surface, which was anodic oxidized without HF (defined as Au/Ti). The geometric area of different electrodes was well controlled to be constant by maintaining the immerged Ti substrate at ca. 1.5 cm^2 throughout the experiments.

2.4. Immobilization of Cyt *c* on Au NCs-TiO_2 NTs/Ti. The as-prepared Au NCs-TiO_2 NTs/Ti was immersed in 10

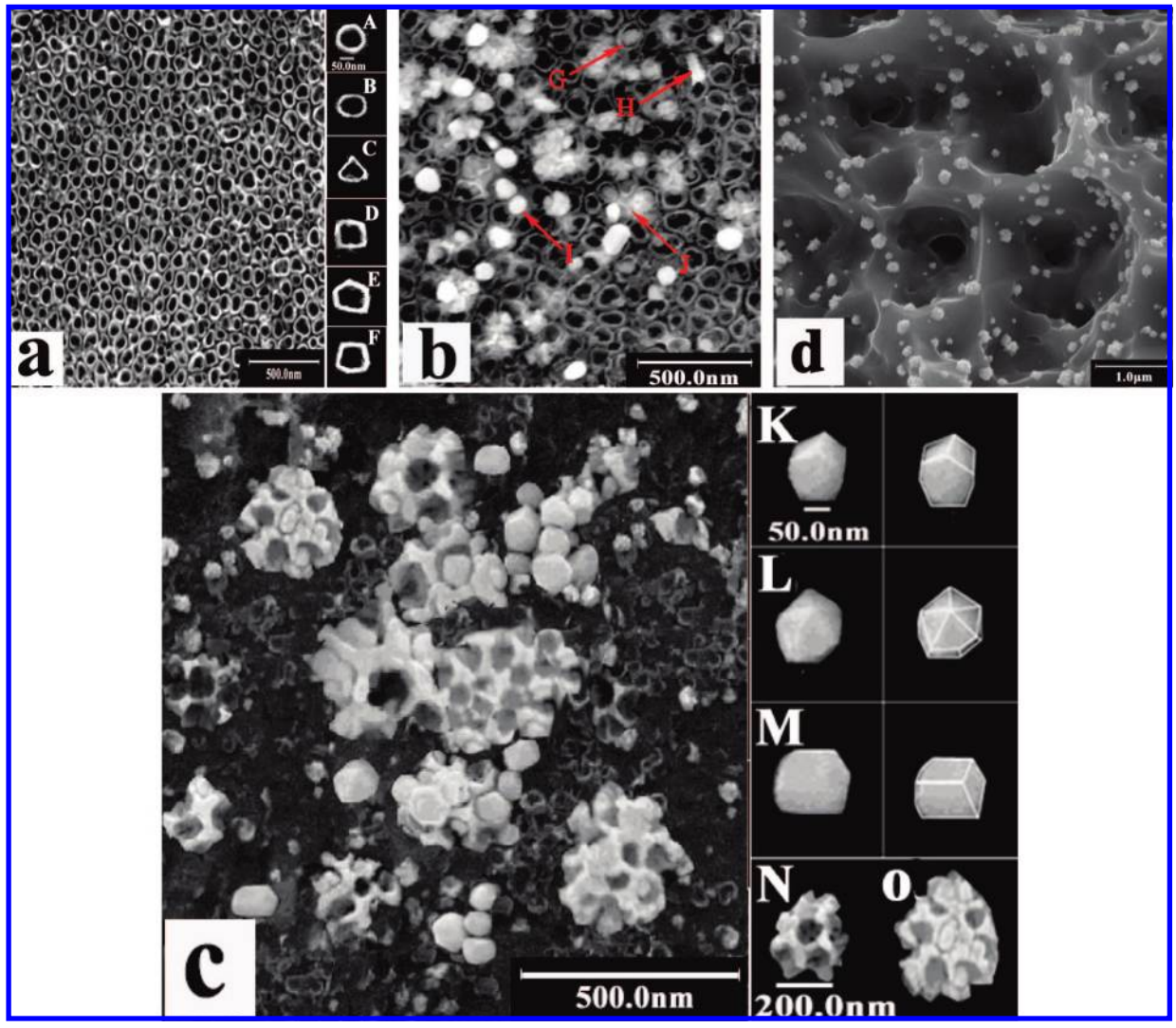

Figure 1. SEM image of the growth and structures of Au NCs in TiO_2 NTs: (a) various shapes of TiO_2 NTs (A−F); (b) Au NCs growth in (G), outside (H), on the top of (I), and between (J) the NTs; (c) various shapes of Au NCs (K−O); and (d) Au in Ti electrode.

μmol·L^{-1} Cyt *c* in 0.1 mol·L^{-1} PBS (pH 6.86) at 4 °C overnight to acquire the Cyt *c*/Au NCs-TiO_2 NTs/Ti electrode. Then, the Cyt *c*/Au NCs-TiO_2 NTs/Ti electrode was removed from the Cyt *c* solution and washed thoroughly with distilled water to remove the unadsorbed Cyt *c* molecules. For comparison, Cyt *c*/Au/Ti was also prepared under the same condition as the preparation of Cyt *c*/Au NCs-TiO_2 NTs/Ti. When they were not used immediately, the modified electrodes were stored at 4 °C in a refrigerator.

2.5. Bioelectrochemistry Experiment. The electrochemical experiments were carried out with a CHI760B electrochemical workstation (CH Instruments, USA) with Au NCs-TiO_2 NTs/Ti or Cyt *c*/Au NCs-TiO_2 NTs/Ti as the working electrode, a platinum electrode as the counter electrode, and a saturated calomel electrode (SCE) as the reference electrode. Buffers were purged with high-purity nitrogen for at least 30 min before experiments, and a nitrogen environment was then kept over solutions in the cell to protect the solution from oxygen. All experiments were performed at room temperature (20 ± 2 °C).

Cyclic voltammetry was used to study the direct electrochemical behavior of Cyt *c* and the biosensing of Cyt *c*/Au NCs-TiO_2 NTs/Ti toward H_2O_2, and an amperometric $i-t$ curve was also used to determinate H_2O_2.

3. Results and Discussion

3.1. Bottom-to-Top Growth, Structures and Electrochemical Activity of Au NCs on in Situ Prepared Vertically Aligned TiO_2 NTs Based on Ti Substrate. An SEM image of the morphology of TiO_2 NTs synthesized by anodic oxidation was shown in Figure 1a. Vertically and compactly arranged TiO_2 NTs have formed on Ti substrate (defined as TiO_2 NTs/Ti). These nanotubes are highly ordered, and vertically aligned, with the tube diameter range from 50 to 90 nm. And the thickness of the tube wall is from 10 to 15 nm. The shapes of the tubes are multiplicate, such as round (Figure 1a, A), elliptical (Figure 1a, B), triangular (Figure 1a, C), quadrangular (Figure 1a, D), pentagonal (Figure 1a, E), and hexagonal (Figure 1a, F), mainly in triangle, round, and ellipse.

Potentiostatic deposition was used to load Au NCs in vertical TiO_2 NTs. According to the cyclic voltammogram of Ti and TiO_2 NTs/Ti in 1% (w/w) $HAuCl_4$+0.02 mol·L^{-1} H_2SO_4 (Figure 2), the reductive peak potential of Au on Ti substrate is around −0.4 V (Figure 2, curve 1), while that on TiO_2 NTs is more positive than −0.2 V (Figure 2 curve 2). Obviously, it is easier for Au to be deposited on the TiO_2 NTs at more positive potentials. Thus, we applied −0.20 V as the deposition potential to obtain the Au loaded TiO_2 NTs/Ti electrode (Au NCs-TiO_2

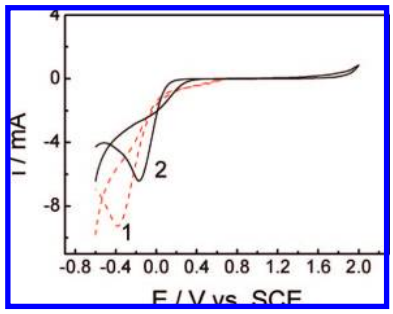

Figure 2. CVs of Ti (1) and TiO_2 NTs/Ti (2) in 1% (w/w) $HAuCl_4$ + 0.02 mol·L^{-1} H_2SO_4.

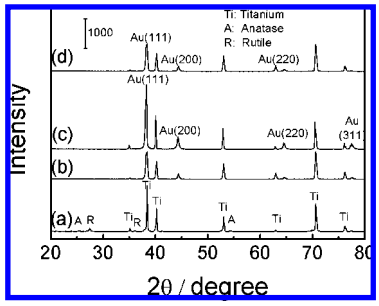

Figure 3. X-ray diffraction pattern of TiO_2 NTs/Ti (a), Au NCs-TiO_2 NTs/Ti before (b) and after (c) slightly removing the NTs, and Au/Ti (d).

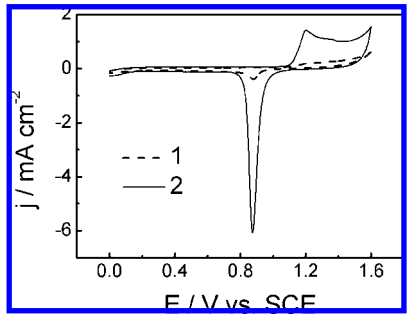

Figure 4. CVs of Au/Ti (1) and Au NCs-TiO_2 NTs/Ti (2) with the same deposition time (1800 s) of Au in 0.5 mol·L^{-1} H_2SO_4.

NTs/Ti) and −0.40 V to obtain the Au/Ti electrode. Panels b and c of Figure 1 show the SEM images of Au NCs-TiO_2 NTs/Ti before and after partial removal of NTs. From the SEM images, we could presume the growth process of Au in TiO_2 NTs/Ti is as follows (as described in Scheme 1). Maybe, due to the intensities of electric fields being comparatively high between and at the bottom of the tubes, Au crystals priorly grew at these regions (as shown in Scheme 1, top and side view 2). As the deposition process went on, more and more Au filled the gaps in and between the tubes gradually, resulting in the formation of some nanorod-like Au restricted in the NTs (Figure 1b, G), some caps with various shapes over the top of the tubes (Figure 1b, H and I), and some crystals filling the gaps between the tubes (Figure 1b, J). If the NTs were removed partially by 0.2 mol·L^{-1} HF, Au nanorods deposited in the tubes and the caps over the top of the tubes would be partially observed (Scheme 1, top view 4 and side view 5), indicating that their shapes were similar to that of the NTs owing to the tubular restriction. As illustrated in Figure 1, some formed polyhedron caps such as pentagonal prism (Figure 1c, K), dodecahedron (Figure 1c, L), and so on. Some formed nanorods like quadrilateral prism (Figure 1c, M) and cylinder. Au deposited between the tubes could grow into the honey-cave-like nanocages with hollows ranging from 50 to 100 nm in diameter (Figure 1c, N−O), which was similar to reports in the literature by Yang et al.[39] Interestingly, we could also observe that the nanocages and nanorods were combined, forming certain kinds of cage-rod hybrid structures, as shown in Figure 1c, O. For comparison, Figure 1d shows that the Ti electrode surface is covered with compact oxide film, and is cross-linked after anodic oxidation without HF, exhibiting a three-dimensional pore network, which is in an ordered and open state and consequently is favorable for Au nanoclusters to distribute or insert. Au nanoparticles in the cluster form are distributed uniformly around the pore canals on the surface of Ti support and the size of the particles is between 100 and 160 nm. The Au clusters separate from each other and are fully exposed.

Figure 2 shows the XRD characterization of TiO_2 NTs and Au NCs on them. After being annealed at 500 °C for 5 h, the TiO_2 NT array consists of a rutile phase ($2\theta = 27.5°$ and 36.1°) and an anatase phase ($2\theta = 25.2°$ and 54.2°) titania, besides the major titanium crystal (Figure 2a). When Au NCs grow in the NTs, the diffraction peaks observed at $2\theta = 38.18°$, 44.39°, 64.58°, and 77.55° correspond to Au (111), Au (200), Au (220), and Au (311), which indicates that due to the oriented effect of TiO_2 NTs as templates, the growing Au NCs have various index facets, besides the normal (111), (200) facets, comparative high-index facets such as (220), (311) are also enclosed. We could also observe that the diffraction peak intensities of (111) and (200) facets are comparatively strong, while the intensities of (220) and (311) are weak, indicating that the Au crystal preferentially forms at (111) and (200) facets (Figure 2b). After the NTs are removed partially by HF, Au in the NTs is exposed, and the intensity of each Au peak is increased obviously (Figure 2c). Moreover, according to the Scherrer formula ($D = k\lambda/[\beta \cos \theta]$), the average diameter (D) of Au NCs can be calculate to be 21.9 nm by the strongest peak of the (111) facet, and by the peak of the (200) facet, D is obtained to be 18.9 nm. This indicates that the Au NCs are mainly in ellipse. However, the size of the Au NCs characterized by XRD is smaller than that obtained by the SEM image. This can be ascribed to the fact that powder XRD is sensitive to the size of coherent scattering domains that can significantly differ from the particle size in the case of mesocrystals composed of smaller primary nanoparticles.[40,41] For comparison, XRD characterization of Au in Ti before anodic oxidation was also investigated (Figure 2d). Similar to Au NCs-TiO_2 NTs/Ti, the diffraction peaks observed at 38.18°, 44.39°, and 64.58° were also observed, indicating the (111), (200), and (220) crystal facets of Au. However, the (311) crystal facet did not appear, due to the nanocluster structure of Au on Ti. Thus, Au NCs in NTs with multiple microstructures and comparatively higher index facets may exhibit better electrochemical activity compared with nanocluster Au on Ti. This might be because the high-index facets have a high density of atomic steps, ledges, and kinks, which can serve as active sites for breaking chemical bonds.[42]

To investigate the electrochemical activity of Au NCs deposited on TiO_2 NTs, we controlled the deposition time of Au on Ti and TiO_2 NTs and investigated the CV response of Ti and TiO_2 NTs/Ti in 0.5 mol·L^{-1} H_2SO_4 after the deposition procedure. As shown in Figure 4, an anodic peak can be observed at 1.20 V for both the Au/Ti and Au NCs-TiO_2 NTs/Ti electrodes. However, the peak current density of Au NCs-TiO_2 NTs/Ti is much higher than that of Au/Ti based on the same surface area (1.5 cm^2). A cathodic peak for Au NCs-TiO_2 NTs/Ti locates at 0.87 V, with the peak current density around −5.82 mA·cm^{-2}, while for Au/Ti the cathodic peak potential

SCHEME 1: Schematic Illustration for the Growth of Au NCs in TiO_2 NTs: (a) Side View and (b) Top View

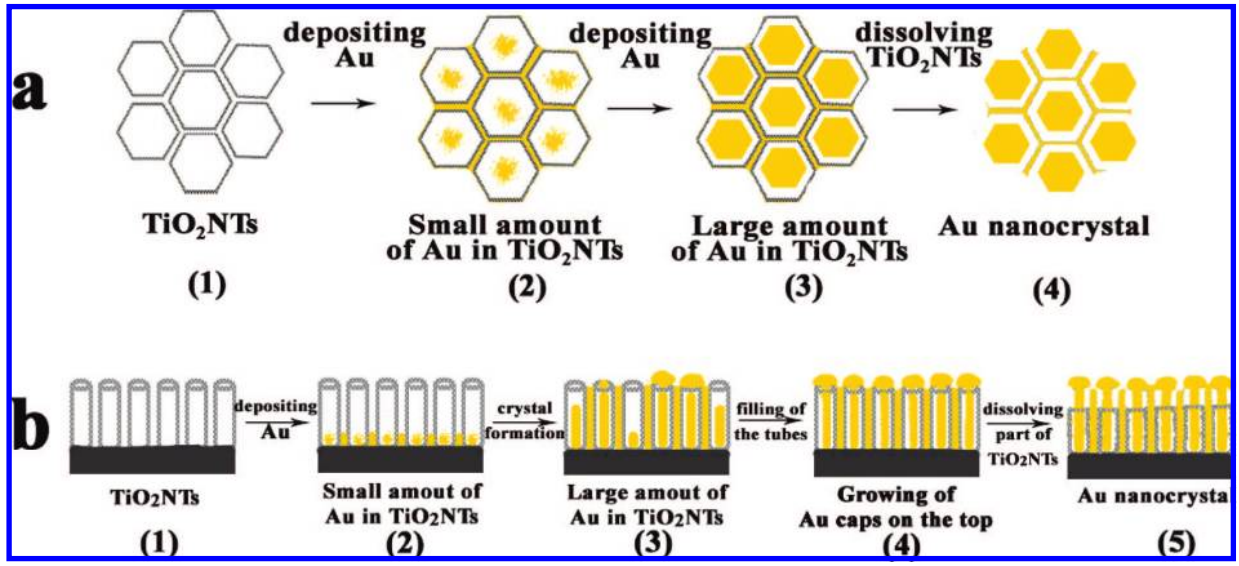

is 0.85 V, with the peak current density of -0.05 mA·cm^{-2}. These results demonstrate that because of larger surface area and higher space freedom compared with Ti, TiO_2 NTs can provide more available free spaces and active sites for the reduction of Au. Thus, a larger deposition amount can be obtained. Meanwhile, due to the template effect of TiO_2 NTs, the deposited Au NCs with multiple nanostructures may expose more electrochemically active sites compared with the nanocluster Au on Ti. Therefore, the Au NCs-TiO_2 NTs electrode exhibits higher peak currents. Moreover, according to the Laviron equation[35,43] the amount of the deposited Au that exhibits electric activities can be calculated to be 2.30×10^{-8} mol·cm^{-2} for Au NCs-TiO_2 NTs/Ti and 9.93×10^{-10} mol·cm^{-2} for Au/Ti. To calculate the real deposition amount, Faraday's law was used. And the deposition cure was also taken into account. The deposition amounts are 3.05×10^{-8} mol·cm^{-2} for Au NCs on TiO_2 NTs/Ti and 1.11×10^{-9} mol·cm^{-2} for Au on Ti. Electrochemical impedance spectroscopy (EIS) was also used to characterize the surface coverage ratio (θ) of Au on Ti and TiO_2 NTs[44,45] (Supporting Information, Figure S1) by using the equation $\theta = 1 - (R_{ct}^0/R_{ct})$, R_{ct}^0 and R_{ct} are the charge transfer resistance values for bare and Cyt *c*-modified electrode, respectively. By increasing or decreasing the charge transfer resistance, the percentage presenting the surface active sites of the electrodes covered by protein molecules was calculated. And the values are 58.1% for Au deposited on Ti and 69.3% for Au deposited on TiO_2 NTs. Obviously, the surface coverage percentage of Au on TiO_2 NTs is lager than that on Ti, which is also in accord with the result deduced from surface coverage calculated by the Laviron equation. As the deposition time went on, CV response of Au increased obviously, showing that the deposition amount and surface coverage of Au increased, which indicates that TiO_2 NTs are favorite for successive deposition of Au, and can provide a higher deposition amount compared with that for Ti (Supporting Information, Figure S2). For further comparison, CV responses of Au with the same deposition amount on TiO_2 NTs and on Ti were measured (Supporting Information, Figure S3). Meanwhile, the CV response of the pure Au disk electrode was also observed. The cathodic peak current density of Au NCs on TiO_2 NTs is larger, and the peak potential is more positive (ca. 0.87V), compared with those of Au on Ti and the pure Au disk electrode. These results demonstrate that the highly dispersed nanostructure Au NCs on TiO_2 NTs exhibits the best electrochemical activity among the three electrodes. All these data are listed in Table 1.

TABLE 1: Comparison of the Electrochemical Activities of Three Electrodes and the Direct Electrochemistry of Cyt *c* on Them

	Au NCs-TiO_2 NTs/Ti	Au/Ti	Au disk
deposition amount of active Au (mol·cm^{-2})[a]	2.30×10^{-8}	9.93×10^{-10}	
cathodic peak current density (mA·cm^{-2})[b]	−5.82	−2.91	
cathodic peak potential of Au (V)	0.87	0.85	0.84
R_{ct} (Ω)	15	18	12
immobilized Cyt *c* redox peaks[c]	+	+	−
Γ (mol·cm^{-2})	1.09×10^{-10}	7.73×10^{-11}	
ΔE (V)	0.096	0.102	
k_s (s^{-1})	1.04	0.142	
dissolved Cyt *c* in the solution redox peaks[c]	+	−	−
Γ* (mol·cm^{-2})	9.33×10^{-12}		
ΔE_p (V)	0.125		
k_s (s^{-1})	0.815		

[a] With the same deposition time (1800 s). [b] With the same real deposition amount (3.05×10^{-8} mol·cm^{-2}). [c] (+) can be observed; (−) cannot be observed.

3.2. Contact Angle of Cyt *c* on the Electrodes. An adsorbed protein molecule may change its conformation to some extent because of protein−surface interactions. Thus, the surface properties will affect the adsorption and activity of proteins. It is known that the improvement in hydrophilicity enhances the biocompatibility of the nanostructure surface for the immobilization of proteins, thereby preserving their natural structure and bioactivity.[46] The surface wettability of TiO_2 NTs/Ti and Au NCs-TiO_2 NTs/Ti was studied by conventional sessile drop contact angle measurements. The contact angle (CA) of the water drop on Au/Ti is 105°, but for Au NCs-TiO_2 NTs/Ti, the CA is 65°, suggesting that compared with Au/Ti, the surface of Au NCs-TiO_2 NTs/Ti is more hydrophilic. This is largely

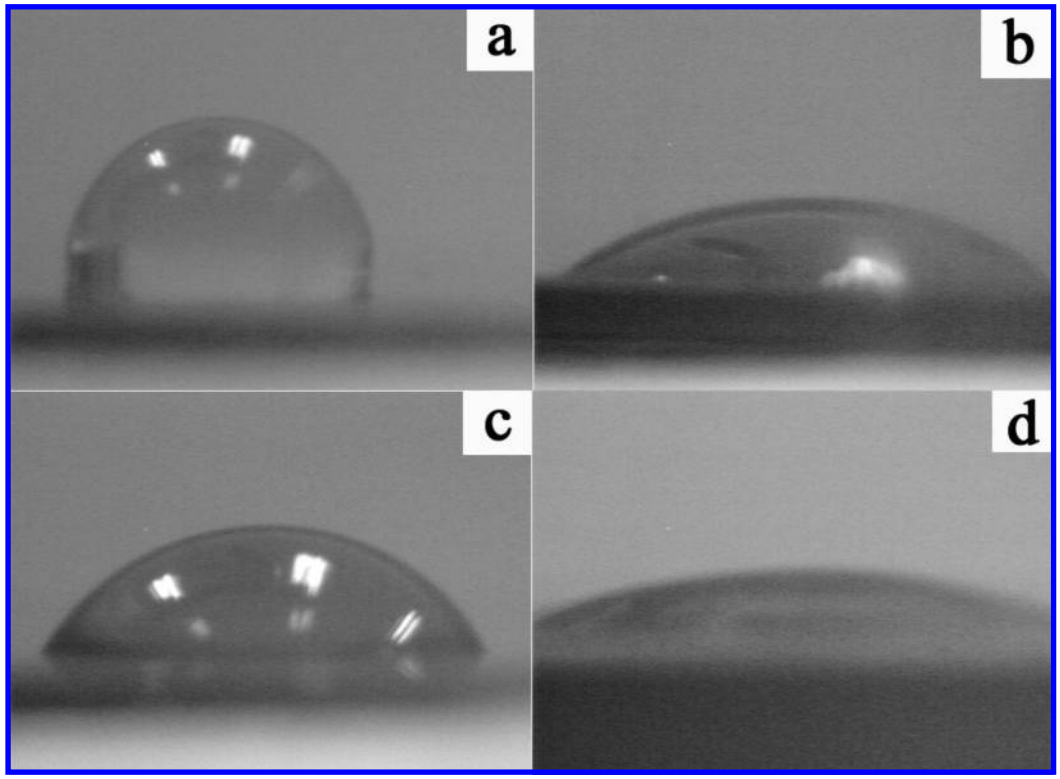

Figure 5. Contact angles of 10 μmol·L^{-1} Cyt *c* solution drops obtained on (a) Au/Ti, (b) Au NCs-TiO_2 NTs/Ti, (c) Ti, and (d) TiO_2 NTs/Ti. The drop volume for Cyt *c* is 5 μL.

due to the excellent hydophilicity of TiO_2 NTs. Because of the formation of the compact oxide layer, the CA of the water drop on Ti (ca. 55°) is larger than that of pure clean metal.[47] However, the CA of the water drop on TiO_2 NTs/Ti (ca. 15°) is much smaller. It is obvious that the formation of TiO_2 NTs can enhance the hydrophilicity of the surface and thus it is significantly convenient for the polar solvent-like $HAuCl_4$ solution to enter and wet the inner surface of the nanotubes. A convenient deposition process may accordingly be realized. Meanwhile, CAs of the Cyt *c* solution on four different surfaces were also analyzed. Panels a and b of Figure 5 display CAs of 10 μmol L^{-1} Cyt *c* solution drops on Au/Ti surface, and on Au NCs-TiO_2 NTs/Ti surface. Similar to water drops, the former (ca. 92°) is larger than the later (ca. 35°), due to the favorable hydrophilicity of TiO_2 NTs (as shown in Figure 5d). It is known that protein molecules consist of hydrophilic and hydrophobic groups. Under biological conditions, the hydrophilic groups of the protein, such as amido and carboxyl, are exposed to the environment and the hydrophobic groups are embedded in the inner core.[48] Thus, they can easily adsorb to the hydrophilic surfaces. The CA of Cyt *c* solution on Au NCs-TiO_2 NTs/Ti is about 35°, which indicates that this surface is an ideal one for Cyt *c* immobilization, and can provide a favorable microenvironment for the maintenance of its activity.

3.3. Direct Electrochemistry of Cyt *c* on Au NCs-TiO_2 NTs/Ti Electrode. The direct electrochemical redox of Cyt *c* immobilized on Au NCs-TiO_2 NTs/Ti was first investigated by cyclic voltammetry, compared with that on Au/Ti. Neither Au/Ti nor Au NCs-TiO_2 NTs/Ti has any peak in 25 mmol·L^{-1} nitrogen-saturated PBS (pH 6.86). But after the immobilization of Cyt *c*, a pair of redox peaks can be observed on both Au/Ti and Au NCs-TiO_2 NTs/Ti (Figure 6, curves A and B), which could not be observed on either TiO_2 NTs or pure Au disk electrode (Surpporting Information, Figure S5). On Au/Ti, a weak anodic peak of Cyt *c* locates at 0.156 V, while a cathodic

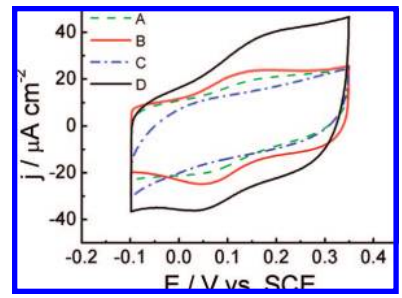

Figure 6. CV responses of Cyt *c*/Au/Ti (A) and Cyt *c*/Au NCs-TiO_2 NTs/Ti (B) in 25 mmol·L^{-1} PBS (pH 6.86), CVs of Au/Ti (C), and Au NCs-TiO_2 NTs/Ti (D) in 10 μmol·L^{-1} Cyt *c* solution.

peak appears at 0.054 V. The peak potential separation (ΔE_p) is 0.102 V, indicating a quasireversible process of Cyt *c* on the Au/Ti electrode. But, as shown in Figure 6, curve B, Cyt *c*/Au NCs-TiO_2 NTs/Ti exhibits a comparatively well-defined pair of redox peaks, located at 0.141 and 0.045 V, respectively. The peak separation (ΔE_p) is 0.096 V, suggesting that the reversibility of Cyt *c*/Au NCs-TiO_2 NTs/Ti is better than that of Cyt *c*/Au/Ti. The anodic and cathodic peaks are almost symmetrical. And the peak current densities are found to be higher compared with the CV response of Cyt *c*/Au/Ti. The results demonstrate that AuNCs-TiO_2 NTs/Ti is advantageous for the direct electrochemistry of Cyt *c* on the surface of the electrode. The immobilization amount (namely average surface coverage, Γ) of electroactive Cyt *c* on Au NCs-TiO_2 NTs/Ti and Au/Ti could be calculated to be 1.09×10^{-10} and 7.73×10^{-11} mol·cm^{-2}, respectively, by the Laviron equation. Furthermore, the surface coverage calculated for a fully packed monolayer of Cyt *c* is 3.40×10^{-11} mol·cm^{-2}, taking the molecule of Cyt *c* as a sphere of 25 Å diameter.[48] Obviously, the surface coverage was higher than monomolecular layer adsorption, and could be presumed to be a multilayer adsorption. It is known that the

isoelectric point (pI) of Cyt *c* is ca. 10.3−10.8,[49,50] and the point of zero charge (p.z.c.) of TiO_2 NTs is ca. 3.[17] In PBS solution (pH 6.86), Cyt *c* is positive charged, and TiO_2 NTs are negative charged. Thus, part of the Cyt *c* molecules were adsorbed on the surface of nanosized Au by the thiol−Au covalent bond, some by natural adsorption, and some by electrostatics on TiO_2 NTs. Furthermore, the percentages of the surface active sites of Au/Ti and AuNCs-TiO_2 NTs/Ti covered by protein molecules, defined as surface coverage (θ), were also calculated through EIS[44,45] (Supporting Information, Figure S1). And the values can be calculated to be 77.6% for Cyt *c* on Au/Ti and 89.5% for Cyt *c* on Au NCs-TiO_2 NTs/Ti, respectively.

Our work also studied the direct electrochemistry of dissolved Cyt *c* in PBS (pH 6.86) solution. In this case, no redox peak of Cyt *c* was found on Au/Ti as usual (Figure 6, curve C). This is because Cyt *c* is a kind of macromolecular protein. Its redox groups are surrounded by a polypeptide chain, which has hindered the electron transfer between themselves and electrodes. Moreover, due to its extremely slow electron-transfer kinetics at the electrode/solution interface, Cyt *c* dissolved in the solution usually shows a short-lived and transient response on conventional electrodes.[1,35,51] Nevertheless, it is interesting that on Au NCs-TiO_2 NTs/Ti, a well-defined CV response is observed amazingly (Figure 6, curve D). This response was observed immediately upon introducing Cyt *c* solution into the electrochemical cell. And the anodic and cathodic peaks appear at 0.10 and 0.225 V, respectively, with the ΔE_p of 0.125 V, indicating a quasireversible process. Compared with Au/Ti, Au NCs-TiO_2 NTs/Ti obviously displays better promotion for the direct electrochemistry of Cyt *c*. This is mainly due to the effect of highly dispersed nanostructure Au in TiO_2 NTs, which can provide a larger surface area and a better environment for the adsorption and electron transfer of Cyt *c* in solution. As shown in Figure 1d, the size of Au on Ti substrate is large, and in the form of clusters, without multiple structures. Thus, the promotion of Au/Ti for macromolecule proteins is relatively weak. No good redox response can be observed. But as for the TiO_2 NTs formed on the Ti substrate, they can provide a large inner surface area and an ideal template for the deposition of Au, which is accordingly highly dispersed and grows into multiple nanostructures. Therefore, the surface area and surface energy of the electrode are increased, and more active sites are exposed. Furthermore, the contact angle mentioned above also demonstrates that the Au NCs-TiO_2 NTs/Ti possesses better hydrophilicity, and thus is advantageous for the adsorption of proteins, which can easily access the surface of the electrode and achieve further direct electrochemical reactions.

Further study investigated the comparison of the CV responses for Cyt *c* dissolved in the solution and immobilized on Au NCs-TiO_2 NTs/Ti. As shown in Figure 6, curve B, for the immobilized Cyt *c*, the anodic peak shifts slightly to the negative potential and the cathodic peak shifts to the positive potential. The redox peaks are more symmetrical compared with the CV of Cyt *c* dissolved in solution, and the reversibility of the electrochemical process increases. The result shows the immobilization of protein on AuNCs-TiO_2 NTs/Ti is indeed suitable for the direct electrochemistry of Cyt *c*. Meanwhile, as mentioned above, the immobilization amount (Γ) of Cyt *c* on Au NCs-TiO_2 NTs/Ti was caculated to be 1.09×10^{-10} mol·cm^{-2} by using the Laviron equation. However, for the direct electrochemical process of Cyt *c* dissolved in solution, the adsorption amount (Γ^*) of Cyt *c* from the solution to the Au NCs-TiO_2 NTs/Ti surface during the electrochemical reaction (Figure 6, curve D) is calculated to be 9.33×10^{-12} mol·cm^{-2} according to the chronocoulometry method.[52] By comparing these two values (1.09×10^{-10} and 9.33×10^{-12} mol·cm^{-2}), it is obvious that the immobilization amount (Γ) is much larger than the adsorption amount. Although the surface adsorption or immobilization amounts of Cyt *c* on the electrode did not show a direct relationship with the electron transfer rate, they may affect the distance between the active center of protein and the electrode. Thus, the electron transfer rate of Cyt *c* is higher when immobilized, with the increase of peak current density, while in solution, affected by the electric double layer, the distance between Cyt *c* and the electrode is larger, with a relatively slower electron transfer rate. Thus, the CV response of dissolved Cyt *c* exhibits lower current density. Meanwhile, due to the comparatively high interface resistance, the charge current exhibits a higher value. Nonetheless, the direct electrochemistry of dissolved Cyt *c* can also be observed, which is hard to realize on other conventional electrodes. It mainly ascribes to the fast adsorption of Cyt *c* on Au NCs, which can also provide fast electron transfer channels. Anyway, due to the enhanced electrochemical activity of highly dispersed Au NCs, the direct electrochemistry of Cyt *c* could be realized on AuNCs-TiO_2NTs/Ti both dissolved in the solution and immobilized on the electrode.

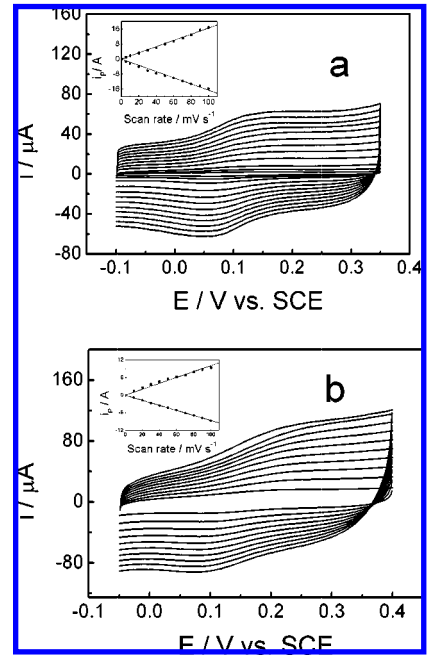

Figure 7. (a) CV responses of Cyt *c*/Au NCs-TiO_2 NTs/Ti in 25 mmol·L^{-1} PBS (pH 6.86) and (b) CVs of Au NCs-TiO_2 NTs/Ti in 25 mmol·L^{-1} PBS (pH 6.86) containing 10 μmol·L^{-1} Cyt *c* solution with different scan rates (v = 2−100 mV·s^{-1}). Insets: Plot of anodic and cathodic peak currents versus the scan rate.

Figure 7a shows the CV response of Cyt *c* modified Au NCs-TiO_2 NTs/Ti in PBS (pH 6.86) with different scan rates. It exhibits an adsorption controlled process, with the peak currents of anodic and cathodic peaks increasing linearly with the scan rates varying from 2 to 100 mV·s^{-1}. The regression equations for anodic and cathodic peak are i_{Pa} (μA) = 0.165v mV·s^{-1} and i_{Pc} (μA) = −0.166v mV·s^{-1}, respectively. Similarly, the voltammetric response of 10 μmol·L^{-1} Cyt *c* on Au NCs-TiO_2 NTs/Ti with different scan rates is displayed in Figure 7b. In the scan rate range of 10−100 mV·s^{-1}, the anodic and cathodic peak currents were both found to be linearly proportional to the scan rates with a correlation coefficient of 0.999 (the inset of Figure 7b), which also corresponds to an adsorption controlled

process. And the regression equations for anodic and cathodic peak are i_{Pa} (μA) = 0.101v mV·s^{-1} and i_{Pc} (μA) = −0.086v mV·s^{-1}, respectively.

To investigate the facile electron transfer, the rate constant of the electrochemical process (k_s) and the anodic and cathodic transfer coefficients (α_a and α_c) were estimated by using the model of Laviron for a surface-controlled electrode process, where k_s = 0.815 (α_a = 0.61, α_c = 0.39) and 1.04 s^{-1} (α_a = 0.55, α_c = 0.45) for Cyt *c* dissolved in solution and immobilized on Au NCs-TiO_2 NTs/Ti, respectively. However, k_s for Cyt *c* immobilized on Au/Ti was only 0.142 s^{-1}, much smaller than that immobilized on Au NCs-TiO_2 NTs/Ti. Moreover this value was even smaller than that for the dissolved Cyt *c* on Au NCs-TiO_2 NTs/Ti. Thus, it is obvious that Au NCs-TiO_2 NTs composite indeed enhanced the electron transfer of Cyt *c* on the surface of the electrode.

Undoubtedly, experimental results indicate that Au NCs not only greatly enhance the electrochemical redox of Cyt *c*, but also promote the electron transfer rate. We assume the mechanism as follow: Au decorated in the NTs can further enhance the active surface area and surface energy of the tubes which are both available for protein binding over the geometrical area. Thus stronger interaction would take place between the Au NCs and the biomolecules. Moreover, nanosized Au particles serve as many branches coming out from the tube wall. And those Au branches can easily pierce into the shells of the proteins, thus the electron transfer distance between the active centers inside the biomolecules and the electrode is shortened. Meanwhile, Au NCs with several crystal facets may provide a favorable environment for the immobilization of Cyt *c* on the electrode surface. That is because the exposure degree of crystal facets may result in the increase of active sites. One or more facets may be fit for the orientation of Cyt *c*, and thus make the active center closer to the active site of the electrode. Accordingly, the interaction between proteins and the electrode is enhanced, and the electron transfer may be promoted. Overall, in this composite system, Au NCs act as the tunnels for the electrons. All the detailed comparison results are listed in Table 1.

3.4. Bioelectrocatalysis of Cyt *c*/Au NCs-TiO_2 NTs/Ti toward H_2O_2. It was reported that proteins containing heme groups, such as HRP, Cyt *c*, hemoglobin, myoglobin, and hemin, could be used as a biocatalyzer to catalyze the electrochemical reduction of H_2O_2.[53] Thereby, we can develop biosensors based on the Cyt *c*/Au NCs-TiO_2 NTs/Ti composite electrode.

Biocatalysis of Cyt *c*/Au NCs-TiO_2 NTs/Ti toward H_2O_2 under neutral circumstance was first investigated. Experiment results indicated that the Cyt *c*/Au NCs-TiO_2 NTs/Ti electrode exhibited a good catalytic activity toward H_2O_2. Figure 8a shows the direct CV response when 1 mmol·L^{-1} H_2O_2 was added into 25 mmol·L^{-1} PBS (pH 7). The Cyt *c*/Au NCs-TiO_2 NTs/Ti electrode showed sensitive responsed to H_2O_2. The cathodic peak currents increased from −8 μA to −10 μA with minor injection of H_2O_2, and increased linearly with the concentration of H_2O_2 in the range of 0.01−10 mmol·L^{-1}. Meanwhile, the peak potentials shift gradually to the negative potentials. The linear regression equation of catalytic currents vs H_2O_2 concentrations can be obtained from the experimental data, which is i_{Pc} (μA) = −0.21 − 0.15c mmol·L^{-1}. If the concentration increases further, the extent of increase of the peak currents is reduced, and they are not linearly proportional to the concentrations.

The biocatalytic reduction property of Cyt *c* to H_2O_2 brings the possibility of a detection method to the quantity of H_2O_2 in solution. The amperometric response of Cyt *c*/Au NCs-TiO_2 NTs/Ti to H_2O_2 was investigated through successive addition of H_2O_2 to a continuously stirred PBS solution (Figure 8b). A potential of 0.02 V was applied to the working electrode. It can be observed that the rapid response takes place within 5 s, and the reduction current at the electrode is proportional to the concentration of H_2O_2 in the range from 2 × 10^{-6} to 3.49 × 10^{-4} mol·L^{-1} (r = 0.999) according to the calibration curve (Figrue 8b, inset). The regression equation can be obtained to be i (nA) = −30.46 − 0.85c μmol·L^{-1}, and the detection limit is 1.2 × 10^{-6} mol·L^{-1}.

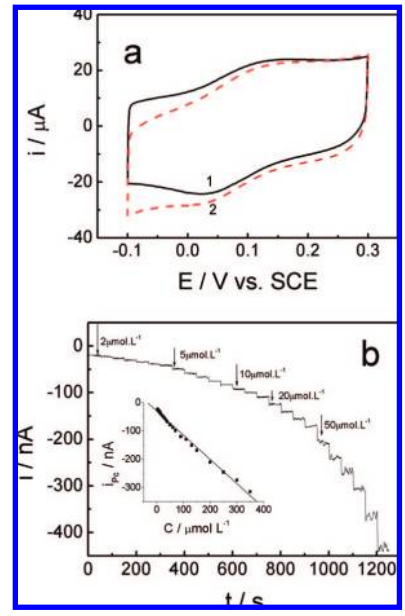

Figure 8. (a) CV response of Cyt *c*/Au NCs-TiO_2 NTs/Ti in 25 mmol·L^{-1} PBS (pH 6.86) (1) and with the addition of 1 mmol·L^{-1} H_2O_2 (2); (b) Current−time plot for the sensor upon successive additions of H_2O_2. Inset: Plot of the relationship between current and H_2O_2 concentration.

Biocompatibility is an important factor that may significantly affect the performance of biosensors. Thus, the biocompatibility of Au NCs-TiO_2 NTs/Ti for Cyt *c* was estimated by Ultraviolet and visible (UV−vis) absorption spectra. The Soret absorption band and Q-band of Cyt *c* were known to be at about 408 and 522 nm (Supporting Information, Figure S6, curve d). When Cyt *c* was directly cast on a quartz substrate, the Soret band was very weak and the peak shape was broad. However, after Cyt *c* was immobilized on the Au NCs-TiO_2 NTs/Ti or Au/Ti, two obvious well-shaped absorption peaks were observed corresponding to the Soret band and Q-band, and no obvious shift in the Soret band was observed (Supporting Information, Figure S6, curves b and c), suggesting that Cyt *c* could retain its native conformation and biological activity after being immobilized on Au NCs-TiO_2 NTs/Ti or Au/Ti electrode, which also enables the direct electron transfer of Cyt *c*.

Furthermore, since the reaction process of heme-containing proteins is affected by protons, and proteins often denature in high or low pH, which greatly limits the application of biosensors, thus pH becomes a remarkable factor for the biosensors.The influence of different pH values on the direct electrochemical redox of Cyt *c* was investigated. Results showed that the bioactivity of Cyt *c* immobilized on Au NCs-TiO_2 NTs/Ti could be well retained in a wide pH range. As shown in Figure 9a, in the range of pH 3−8, the CVs for Cyt *c*/Au NCs-TiO_2 NTs/Ti in PBS exhibited good shapes of redox peaks. As the values of pH increase, both the anodic and cathodic peaks shift negatively. The formal potential $E^{0\prime}$, which was estimated

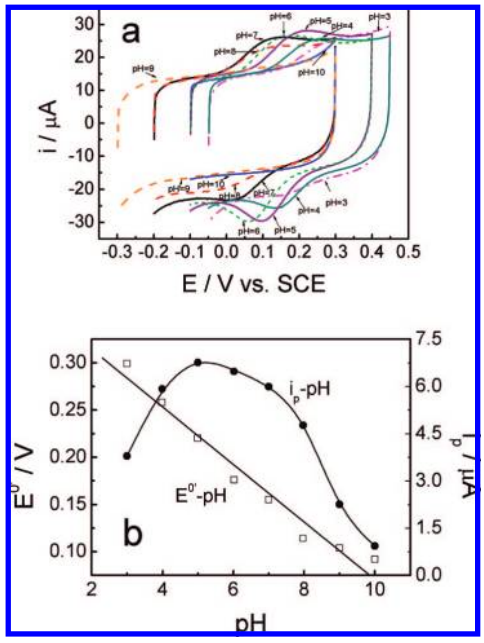

Figure 9. (a) CVs of Cyt *c*/Au NCs-TiO_2 NTs/Ti electrode in PBS at various pH values (pH 3−8) at a scan rate of 50 mV·s^{-1}; (b) effect of pH on formal potentials and peak currents for Cyt *c*/Au NCs-TiO_2 NTs/Ti in 25 mmol·L^{-1} PBS.

as the midpoint of cathodic and anodic peak potentials, had a linear relationship with pH (from 3.0 to 8.0), as shown in Figure 9b, indicating that one proton participated in the electron transfer process.[53] And the peak currents reached a maximum at pH 5. All changes in CV peak potentials and currents with pH were found to be reversible between pH 3 and 8, and when pH is lower than 3 or higher than 8, the redox peaks become inconspicuous, and finally disappear. As mentioned above, in neutral and acidic solution, Cyt *c* is positive charged. And the p.z.c. of TiO_2 NTs is ca. 3. They are negatively charged when pH is higher than 3. Thus, good electrostatic adsorption can take place between Cyt *c* and the Au NCs-TiO_2 NTs/Ti electrode in the pH rage from 3 to 8. Experimental results show that when pH is 5, the best adsorption and orientation of Cyt *c* may be realized. Thus, the highest peak current and best peak shape is accordingly obtained. However, when pH is higher than 8, Cyt *c* will denaturalize. And when pH is lower than 3, extraordinary electrostatic adsorption may take place, which also results in the denaturalization of Cyt *c*. Therefore, the redox peaks gradually disappear. Nonetheless, it is obvious that Cyt *c*/Au NCs-TiO_2 NTs/Ti retains a good stability in a wide pH range. This also means that this biosensor can work in pH conditions varied from 3 to 8. On the basis of these results, amperometric sensing of the electrocatalytic reduction for H_2O_2 in different pH mediums was carried out. The results are displayed in Figure 10. In the range of pH 3−8, stable current−time curves can be obtained. Experiment results show that the pH value only affects the variation of the response currents. But a good signal-to-noise ratio can be obtained under all these pH conditions. Thus, Cyt *c*/Au/TiO_2 NTs/Ti exhibits a good adaptability to the variation of pH in solutions when applied as the H_2O_2 biosensor.

The stability and reproducibility of Cyt *c*/Au NCs-TiO_2 NTs/Ti were also checked, which could be key factors in the development of novel biosensor devices. The electrode showed almost no decrease in voltammetric current when subject to 50 potential cycles from −0.2 to 0.4 V (vs SCE) at a scan rate of 50 mV·s^{-1} in 25 mmol·L^{-1} PBS (pH 6.86). When stored in 25 mmol·L^{-1} PBS (pH 6.86) at 4 °C, the current response was

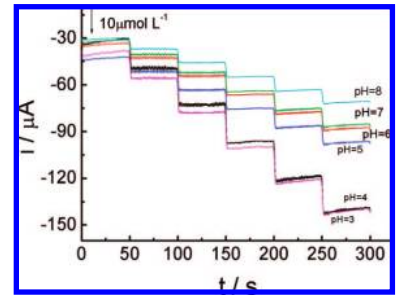

Figure 10. Current−time plot for the sensor upon successive additions of 10 μmol·L^{-1} H_2O_2 in PBS with different pH values (pH 3−8).

found to be stable, and there was no deviation from the initial response. In addition, after 30 days, no obvious decrease in the response to H_2O_2 was observed. The response current could be obtained to be 98.7% of the initial response. In fact, both the nanotubular structure of TiO_2 NTs and the Au NCs provide excellent stability for the biosensor, even in acidic or alkaline solutions. Its high stability and sensitivity effectively made the biosensor display a reasonably longer useable life and more determination times.

4. Conclusions

Ordered TiO_2 NTs based on Ti substrate were in situ synthesized by anodic oxidation in this study. The as-prepared vertically aligned TiO_2 NTs are very suitable and advantageous for further introduction of noble metals compared with plane Ti substrate, because they can provide larger surface area, more active sites, and a favorable surface environment for the electrodeposition. Au was electrodeposited into and among the NTs and the formed hybrid structures of nanonets and nanorods due to the template effect and tubular confinement of TiO_2 NTs. On the basis of multiple microstructures and high dispersion, the resulting Au NCs-TiO_2 NTs composite structure is adapted for the immobilization and direct electrochemistry of Cyt *c*, and Au NCs serves as an excellent electron transfer channel, which enhances the electron transfer rate of Cyt *c* significantly. Because the shape diversity of Au may greatly increase the surface area and surface energy, provide more active sits, and shorten the electron transfer distance between Cyt *c* and the electrode, it accordingly improves the electrochemical performance of the electrode. A pair of redox peaks owing to the direct electron transfer of Cyt *c* was obtained both in Cyt *c* solution and for the immobilized Cyt *c*. This Cyt *c*/Au NCs-TiO_2 NTs/Ti electrode has been applied to electrocatalyze the reduction of H_2O_2 as a biosensor with a detection range from 2×10^{-6} to 3.49×10^{-4} mol·L^{-1}. The effect of pH has also been studied, which exhibits some important impact on the peak potentials and currents of the Cyt *c* and thus plays a critical role in biosensing. A primary insight into the structure-effect relationship of a novel nanostructure electrode has been gained and a promising platform for fabricating the third-generation biosensors has been accordingly provided.

Acknowledgment. This work was supported by the National Natural Science Foundation of China (Project Nos. 20577035 and 50478106), the Nanometer Science Foundation of Shanghai, China (No. 0652nm030), and the Program for Young Excellent Talents in Tongji University (No. 2006KJ060).

Supporting Information Available: Electrochemical impedance spectroscopy (EIS) of Ti, TiO_2NTs/Ti, Au/Ti, Au NCs-TiO_2 NTs/Ti, Cyt *c*/Au/Ti, and Cyt *c*/Au NCs-TiO_2 NTs/Ti

electrodes (Figure S1); CV responses of Au NCs-TiO_2 NTs/Ti with different deposition time in 0.5 mol·L^{-1} H_2SO_4 (Figure S2); CV obtained at Au-Ti, Au NCs-TiO_2 NTs/Ti, and Au disk electrode in 0.5 mol L^{-1} H_2SO_4 solution (Figure S3); contact angles of sessile water drops obtained on Au-Ti, Au NCs-TiO_2 NTs/Ti, Ti, and TiO_2 NTs/Ti (Figure S4); CV responses of Cyt *c*/TiO_2 NTs/Ti and Cyt *c*/Au disk electrode in 25 mmol·L^{-1} PBS (Figure S5); and UV−vis absorption spectra for 10 μmol·L^{-1} Cyt *c* in pH 6.86 PBS and immobilized on a quartz substrate, Au/Ti, and Au NCs/TiO_2 NTs (Figure S6). This material is available free of charge via the Internet at http://pubs.acs.org.

References and Notes

(1) Ding, X.; Yang, M.; Hu, J.; Li, Q.; McDougall, A. *Microchim. Acta* **2007**, *158*, 65–71.

(2) Wang, L.; Wang, E. *Electrochem. Commun.* **2004**, *6*, 49–54.

(3) Jensen, P. S.; Chi, Q.; Grumsen, F. B.; Abad, J. M.; Horsewell, A.; Schiffrin, D. J.; Ulstrup, J. *J. Phys. Chem. C* **2007**, *111*, 6124–6132.

(4) Feng, J. J.; Zhao, G.; Xu, J. J.; Chen, H. Y. *Anal. Biochem.* **2005**, *342*, 280–286.

(5) Xiang, C.; Zou, Y.; Sun, L.-X.; Xu, F. *Talanta* **2007**, *74*, 206–211.

(6) Yin, Y.; Lu, Y.; Wu, P.; Cai, C. *Sensors* **2005**, *5*, 220–234.

(7) Zhao, Y. D.; Bi, Y. H.; Zhang, W. D.; Luo, Q. M. *Talanta* **2005**, *65*, 489–494.

(8) Yin, Y.; Wu, P.; Lü, Y.; Du, P.; Shi, Y.; Cai, C. *J. Solid State Electrochem.* **2007**, *11*, 390–397.

(9) Davis, J. J.; Green, M. L. H.; Allen, O.; Hill, H.; Leung, Y. C.; Sadler, P. J.; Sloan, J.; Xavier, A. V.; Chi Tsang, S. *Inorg. Chim. Acta* **1998**, *272*, 261–266.

(10) Xu, Y.; Liang, J.; Hu, C.; Wang, F.; Hu, S.; He, Z. *J. Biol. Inorg. Chem.* **2007**, *12*, 421–427.

(11) Stoll, C.; Kudera, S.; Parak, J. W.; Lisdat, F. *Small* **2006**, *2*, 741–743.

(12) Dai, Z. H.; Ni, J.; Huang, X. H.; Lu, G. F.; Bao, J. C. *Bioelectrochemistry* **2007**, *70*, 250–256.

(13) Rosales-Hernandez, M. C.; Mendieta-Wejebe, J. E.; Correa-Basurto, J.; Vazquez-Alcantara, J. I.; Terres-Rojas, E.; Trujillo-Ferrara, J. *Int. J. Biol. Macromol.* **2007**, *40*, 444–448.

(14) Wang, J.; Li, M.; Shi, Z.; Li, N.; Gu, Z. *Anal. Chem.* **2002**, *74*, 1993–1997.

(15) Zhao, G. C.; Yin, Z. Z.; Zhang, L.; Wei, X. W. *Electrochem. Commun.* **2005**, *7*, 256–260.

(16) Mu, C.; Zhao, Q.; Xu, D.; Zhuang, Q.; Shao, Y. *J. Phys. Chem. B* **2007**, *111*, 1491–1495.

(17) Bavykin, D. V.; Milsom, E. V.; Marken, F.; Kim, D. H.; Marsh, D. H.; Riley, D. J.; Walsh, F. C.; El-Abiary, K. H.; Lapkin, A. A. *Electrochem. Commun.* **2005**, *7*, 1050–1058.

(18) Xiao, P.; Garcia, B. B.; Guo, Q.; Liu, D.; Cao, G. *Electrochem. Commun.* **2007**, *9*, 2441–2447.

(19) Paulose, M.; Shankar, K.; Yoriya, S.; Prakasam, H. E.; Varghese, O. K.; Mor, G. K.; Latempa, T. A.; Fitzgerald, A.; Grimes, C. A. *J. Phys. Chem. B* **2006**, *110*, 16179–16184.

(20) Zhang, Z.; Yuan, Y.; Shi, G.; Fang, Y.; Liang, L.; Ding, H.; Jin, L. *Environ. Sci. Technol.* **2007**, *41*, 6259–6263.

(21) Quan, X.; Ruan, X.; Zhao, H.; Chen, S.; Zhao, Y. *Environ. Pollut.* **2007**, *147*, 409–414.

(22) Lu, N.; Quan, X.; Li, J.; Chen, S.; Yu, H.; Chen, G. *J. Phys. Chem. C* **2007**, *111*, 11836–11842.

(23) Zhuang, H. F.; Lin, C. J.; Lai, Y. K.; Sun, L.; Li, J. *Environ. Sci. Technol.* **2007**, *41*, 4735–4740.

(24) Li, Q.; Luo, G.; Feng, J. *Electroanalysis* **2001**, *13*, 359–363.

(25) Zhang, Y.; He, P.; Hu, N. *Electrochim. Acta* **2004**, *49*, 1981–1988.

(26) Topoglidis, E.; Cass, A. E. G.; O'Regan, B.; Durrant, J. R. *J. Electroanal. Chem.* **2001**, *517*, 20–27.

(27) Topoglidis, E.; Campbell, C. J.; Cass, A. E. G.; Durrant, J. R. *Langmuir* **2001**, *17*, 7899–7906.

(28) Zhu, B.; Guo, Q.; Huang, X.; Wang, S.; Zhang, S.; Wu, S.; Huang, W. *J. Mol. Catal. A: Chem.* **2006**, *249*, 211–217.

(29) Liu, A.; Wei, M.; Honma, I.; Zhou, H. *Anal. Chem.* **2005**, *77*, 8068–8074.

(30) Macak, J. M.; Aldabergerova, S.; Ghicov, A.; Schmuki, P. *Phys. Status Solidi A* **2006**, *203*, R67−R69.

(31) Yoriya, S.; Paulose, M.; Varghese, O. K.; Mor, G. K.; Grimes, C. A. *J. Phys. Chem. C* **2007**, *111*, 13770–13776.

(32) Macak, J. M.; Schmidt-Stein, F.; Schmuki, P. *Electrochem. Commun.* **2007**, *9*, 1783–1787.

(33) Yang, L.; He, D.; Cai, Q.; Grimes, C. A. *J. Phys. Chem. C* **2007**, *111*, 8214–8217.

(34) Ju, H.; Liu, S.; Ge, B.; Lisdat, F.; Schelle, F. r. *Electroanalysis* **2002**, *14*, 141–147.

(35) Zhong, T.; Qu, Y.; Huang, S.; Li, F. *Microchim. Acta* **2007**, *158*, 291–297.

(36) Wang, Q.; Li, N.; Wu, Y. *Electroanalysis* **2001**, *13*, 149–154.

(37) Liu, H.; Tian, Y.; Deng, Z. *Langmuir* **2007**, *23*, 9487–9494.

(38) Liu, S.; Chen, A. *Langmuir* **2005**, *21*, 8409–8413.

(39) Yang, L.; Cai, Q.; Yu, Y. *Inorg. Chem.* **2006**, *45*, 9616–9618.

(40) Zhong, X.; Feng, Y.; Lieberwirth, I.; Knoll, W. *Chem. Mater.* **2006**, *18*, 2468–2471.

(41) Lee, Y. W.; Kim, N. H.; Lee, K. Y.; Kwon, K.; Kim, M.; Han, S. W. *J. Phys. Chem. C* **2008**, *112*, 6717–6722.

(42) Tian, N.; Zhou, Z.-Y.; Sun, S.-G.; Ding, Y.; Wang, Z. L. *Science* **2007**, *316*, 732–735.

(43) Laviron, E. *J. Electroanal. Chem.* **1979**, *101*, 19–28.

(44) Song, Y. Y.; Li, Y.; Yang, C.; Xia, X. H. *Anal. Bioanal. Chem.* **2008**, *390*, 333–341.

(45) Zuo, G.; Liu, X.; Yang, J.; Li, X.; Lu, X. *J. Electroanal. Chem.* **2007**, *605*, 81–88.

(46) Wu, S.; Ju, H. X.; Liu, Y. *Adv. Funct. Mater.* **2007**, *17*, 585–592.

(47) Balaur, E.; Macak, J. M.; Taveira, L.; Schmuki, P. *Electrochem. Commun.* **2005**, *7*, 1066–1070.

(48) Schlereth, D. D. *J. Electroanal. Chem.* **1999**, *462*, 198–207.

(49) Geng, R.; Zhao, G.; Liu, M.; Li, M. *Biomaterials* **2008**, *29*, 2794–2801.

(50) Kum, M. C.; Joshi, K. A.; Chen, W.; Myung, N. V.; Mulchandani, A. *Talanta* **2007**, *74*, 370–375.

(51) Wu, Y.; Hu, S. *Colloid Surf., B* **2005**, *41*, 299–304.

(52) Osteryoung, R. A. *Prepr.-Am. Chem. Soc., Div. Fuel Chem.* **1967**, 11.

(53) Gu, H. Y.; Yu, A. M.; Chen, H. Y. *J. Electroanal. Chem.* **2001**, *516*, 119–126.

JP712054C